Vol. 04, Iss. 4 (2026) 436-442, DOI: 10.61552/JME.2026.04.002

JME

Journal of Materials and Engineering

www.jme.aspur.rs

Research article

Fabrication and Optical Characterization of UV-Cured Phosphor–Polymer Composite Layers for White LED Packaging

Minh-Duc Vuong[a,b], Hoang-Minh Tran[a,b], Phuc-Khang Nguyen[a,b], Minh-Triet Nguyen[b,c,d], Quang-Khoi Nguyen[b,c] *

[a]*High School for the Gifted, VNU-HCM, Vietnam National University Ho Chi Minh City, Ho Chi Minh City 700000, Vietnam,*
[b]*Vietnam National University Ho Chi Minh City, Ho Chi Minh City 700000, Vietnam,*
[c]*Faculty of Physics and Engineering Physics, VNUHCM-University of Science, Ho Chi Minh City 700000, Vietnam,*
[d]*Faculty of Electronics Engineering 2, Posts and Telecommunications Institute of Technology, Ho Chi Minh City 700000, Vietnam.*

Keywords:

pcW-LED
UV curing
UV LED
Phosphor-silicone
Semiconductor packaging
Composite

* Corresponding author:

Quang-Khoi Nguyen
E-mail: nqkhoi@hcmus.edu.vn

Received: 14 September 2026
Revised: 24 October 2026
Accepted: 10 November 2026

A B S T R A C T

In the semiconductor packaging field, speed, efficiency, and sustainability are key drivers of innovation. This study demonstrated a packaging process using ultraviolet (UV) radiation at wavelength 365 nm for curing resin which is mixed with yellow phosphor in the packaging process of ultraviolet curing resin. Utilize UV radiation curing to quickly cure yellow light conversion layer compared to the traditional thermal drying methods. The optical property and color performance of packaged white LED are investigated. The obtained results highlight the advantages of UV LED technology in enhancing efficiency, reducing costs, and simplifying packaging process compared to thermal curing-based methods. UV LED curing enables the semiconductor packaging industries to transition to a more energy-efficient, environmentally friendly, high-performance solution.

© 2026 Journal of Materials and Engineering

1. INTRODUCTION

In recent decades, phosphor-converted white light-emitting diodes (pc-WLEDs) have emerged as the dominant technology in solid-state lighting (SSL), progressively replacing conventional light sources due to their high luminous efficacy, long operational lifetime, and eco-friendly nature [1-4]. The most commercially prevalent configuration for generating white light couples a high-efficiency indium gallium nitride (InGaN) blue LED chip with a down-converting yellow phosphor matrix

(typically $Y_3Al_5O_{12}:Ce^{3+}$ or YAG:Ce) [5-8]. When electrically biased, the semiconductor die emits primary blue photons. A portion of this blue light is absorbed by the phosphor particles and down-converted into secondary yellow light, while the remaining unconverted blue light passes directly through the encapsulation layer. The optical mixing of these complementary spectral components ultimately yields the perception of high-quality white light to the human eye [9-13]. Despite these advancements, a significant challenge in pc-WLED performance stems from inefficient energy conversion. Only a fraction of the input electrical power is converted into useful light, while the remainder is dissipated as heat at the semiconductor junction and within the phosphor layer due to Stokes shift losses [14-17]. If this localized heat accumulation is not effectively managed, it triggers thermal quenching, which degrades luminous efficiency, induces color shifting, and drastically shortens the device's operational lifespan. Consequently, integrating the pc-WLED onto a high-performance thermal management system (heatsink) via an intermediate substrate or Printed Circuit Board (PCB) is a critical engineering requirement. This assembly facilitates rapid heat conduction away from the active layers and maximizes convective dissipation through the heatsink fins into the ambient environment, thereby ensuring long-term optical stability and device reliability [18-20]. Such a white LED mounted on a heatsink is illustrated in Figure 1.

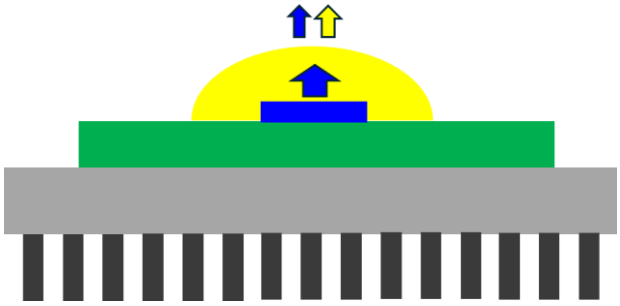


Fig. 1. Principle of phosphor converted white LED and its typically mounting structure on a heatsink.

This study demonstrates an efficient micro-packaging process using 365 nm ultraviolet (UV) radiation for the rapid photopolymerization of a yellow phosphor-resin composite layer, offering a fast alternative to traditional thermal curing methods. The optical properties and color performance of the fabricated pc-WLED are systematically investigated. The results highlight the advantages of UV-curing technology in enhancing throughput, reducing thermal budgets, and simplifying manufacturing flows, thereby presenting an energy-efficient, environmentally friendly, and high-performance solution for the solid-state lighting industry.

2. PACKAGING METHOD FOR PHOSPHOR CONVERTED WHITE LIGHT EMITTING DIODES WITH USING ULTRAVIOLET CURING RESIN

Figure 2 illustrates the sequential schematic flow of a packaging using trasparent molding and ultraviolet (UV) radiation-curing encapsulation process for fabricating phosphor-converted white light-emitting diodes (pc-WLEDs). The packaging procedure is systematically categorized into four core phases. The fisrt one is substrate preparation as shown in Fig. 2(a). The process initiates with a comercial pre-assembled packaging unit consisting of a blue LED excitation source wire-bonded onto a standardized green substrate carrier.

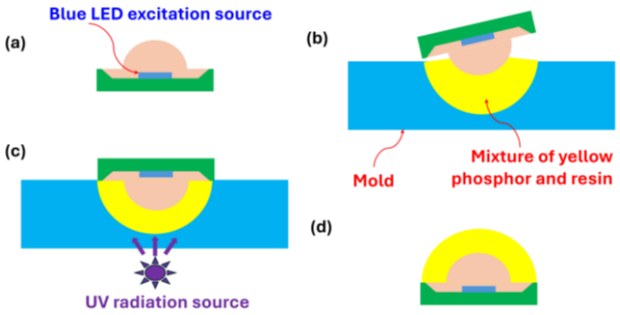


Fig. 2. Main step in packaging process for phosphor converted white light emitting diodes with using ultraviolet radiation for curing.

The second phase is pick and place in the mold with matrix of yellow phosphor and resin as shown in Fig. 2(b). A custom-engineered mold featuring a precise hemispherical cavity is filled with a homogeneous mixture of yellow phosphor and liquid polymer resin. The inverted blue LED substrate assembly is then precisely aligned and mechanically pressed into the mold cavity. This imprinting step forces the liquid phosphor-resin composite to uniformly redistribute around the primary optical dome of the blue LED, ensuring consistent coating thickness.

The third phase is curing step via UV irradiation as shown in Fig. 2(c). While the package remains secured under mechanical compression within

the mold housing, an external UV radiation source delivers high-intensity ultraviolet energy from the lower quadrant. The UV photons penetrate the mold material to initiate a rapid, localized photochemical reaction. This photo-exposure triggers cross-linking within the reactive monomers of the resin, inducing rapid solidification (curing) of the phosphor matrix.

The final step is demolding and device realization as shown in Fig. 2(d). Upon completion of the photopolymerization cycle, the package undergoes a structural release profile to separate the component from the mold cavity. The resulting final pc-WLED architecture exhibits a geometrically precise, solid yellow phosphor layer bonded to the primary blue LED package. Next the optical and color performance of finished package white LED will be tested with spectral meter in the integrating sphere system.

In this study, the UV-resin which can be cured under irradiation wavelength of 365 nm. The yellow phosphor is the type of YAG:Ce3+. the 6 wt% concentration was the ratio of mass of yellow phosphor to the mass of mixture of yellow phosphor and UV-resin. The UV exposure time is 5 mins under UV LED 365 nm to ensure the curing of mixture. The radius of the hemispherical hollow in the mold is 2.5 mm. The molding process is conducted in the room temperature condition. The optical property is measured by the spectrometer of the integrating sphere system. To avoid the thermal effect, sample is driven as small injection current of 50 mA. To make sure the consistency, the at least 3 sample are fabricated and measured.

3. RESULTS

Figure 3 presents optical photographs demonstrating the structural transition of the device during the manufacturing workflow. For the case of pre-packaging state (left photo), the photo shows the unencapsulated blue LED base serving as the primary excitation source, with its bare, transparent hemispherical lens and internal semiconductor die clearly visible. For the case of post-packaging state (right photo), the photo showed the packaged device following the UV-assisted encapsulation sequence, where the primary lens is completely encapsulated by a highly uniform, hemispherical yellow phosphor-resin matrix layer perfectly centered within the housing.



Fig. 3. Photographs demonstrating the structural transition of the device during the manufacturing workflow.

Figure 4 show the electroluminescence (EL) spectrum of the fabricated white light-emitting diode (pc-WLED) prepared with a 6 wt% weight concentration of yellow phosphor in the resin matrix. The spectral power distribution, plotted as a function of wavelength ranging from 360 nm to 830 nm, exhibits a distinct dual-peak profile characteristic of standard phosphor-converted white solid-state lighting architectures. The primary emission peak in the Blue region shows a highly intense, narrow emission band is observed in the short-wavelength region, peaking sharply at approximately 455 nm. This dominant peak originates from the direct radiative recombination of electron-hole pairs within the InGaN-based primary blue LED die excitation source. The secondary broad peak by the phosphor down-conversion show a much broader emission band spans from 500 nm to over 700 nm, reaching its maximum intensity at around 545 nm. This broad spectrum signifies the successful down-conversion mechanism, where a portion of the high-energy blue photons emitted by the die is absorbed by the 6 wt% yellow phosphor layer and re-emitted at lower energies (longer wavelengths emission).

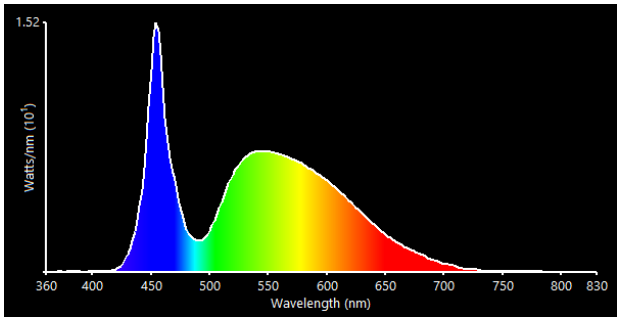


Fig. 4. The electroluminescence (EL) spectrum of the fabricated white light-emitting diode (pc-WLED) prepared with a 6 wt% weight concentration of yellow phosphor in the resin matrix.

The overlapping combination of the unabsorbed, transmitted blue light and the down-converted broad yellow-green light synthesizes the white spectrum with CCT of 6164K. At this specific 6 wt% phosphor loading, the relative intensity ratio between the blue peak and the broad phosphor envelope yields a calculated spectral balance optimized for white light generation.

Figure 5 show the CIE 1931 chromaticity diagram alongside a magnified view of the Planckian locus, evaluating the color quality and performance of the fabricated pc-WLED with a 6 wt% yellow phosphor concentration. The calculated color coordinates (x, y) of the synthesized white light are plotted as a distinct black dot situated in the central white region of the chromaticity space. The coordinate point (x,y) lies at location of (0.32, 0.38). As demonstrated in the magnified inset (right), the coordinate point is positioned adjacent to the Planckian (blackbody) locus line. It aligns closely with the iso-temperature lines between 5500 K and 6000 K, corresponding to a CCT of approximately 6000 K. The proximity of the color point to the blackbody locus confirms that the 6 wt% phosphor loading successfully combine the blue die emission and yellow down-conversion light, yielding a high-quality, stable cool-white light output suitable for standard solid-state lighting applications.

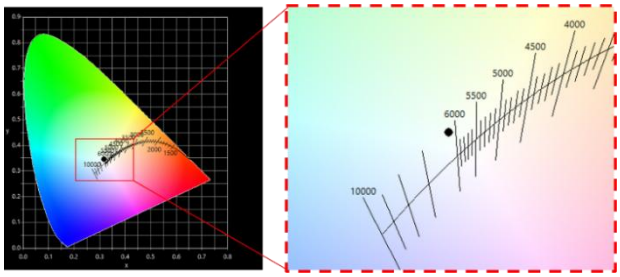


Fig. 5. the CIE 1931 chromaticity diagram alongside a magnified view of the Planckian locus.

A comprehensive evaluation of the color reproduction fidelity was conducted by analyzing the fifteen individual color rendering indices (Figure 6). The fabricated pc-WLED achieves a moderate general color rendering index Ra of approximately 74, indicating acceptable performance for general lighting applications. Across the standard pastel palette R1-R8, the rendering capabilities remain balanced, peaking at R7 (light violet) and R3 (saturated yellowish-green). However, a detailed inspection of the special and saturated color indices reveals a pronounced deficiency in the deep-red spectral region, with the R9 index dropping significantly to a negative value of approximately -25. This phenomenon is a well-documented limitation inherent to conventional mono-phosphor white LEDs that utilize yellow-emitting YAG:Ce 3+ materials, which lack sufficient spectral power density above 600nm. Conversely, the device demonstrates acceptable performance for human skin tone replication, with the caucasian skin (R13) and Asian skin (15) indices reaching approximately 73 and 65, respectively.

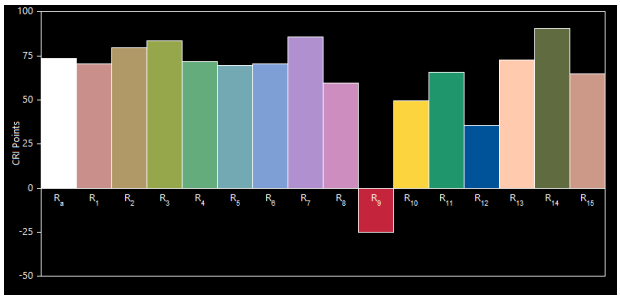


Fig. 6. Difference of the fifteen individual color rendering indices.

To overcome the inherent limitations of the traditional CIE Ra metric, the color rendering properties of the 6 wt% yellow phosphor-converted LED were further analyzed using the advanced IES TM-30-15 method (Figure 7). This framework provides a more comprehensive evaluation through the dual-metric system comprising the Fidelity Index (Rf) and the Gamut Index (Rg), supplemented by a localized color vector graphic across 16 distinct hue bins.

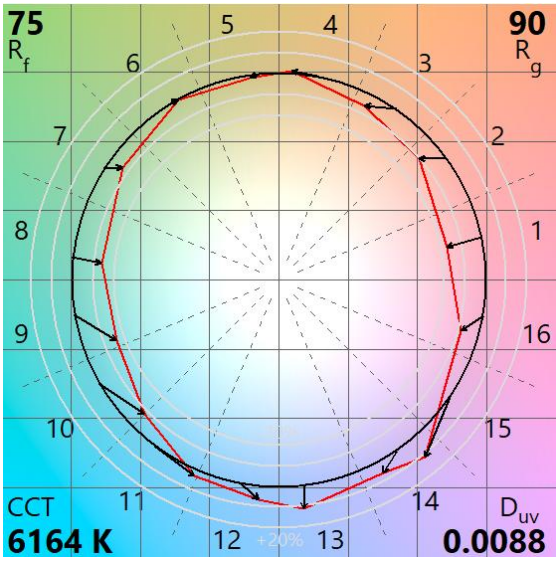


Fig. 7. The color performance of the 6 wt% yellow phosphor-converted LED under IES TM-30-15 evaluation.

The device achieves a Fidelity Index Rf of 75, which closely matches the calculated general CRI Ra approximate 74, reinforcing the acceptable color rendering capabilities under a standard set of 99 color evaluation samples. Concurrently, the Gamut Index (Rg) is recorded at 90. Since Rg < 100, this indicates an overall reduction in color saturation (desaturation) across the synthesized spectrum compared to the reference illuminant.

The advanced calculation establishes a precise CCT of 6164 K, confirming the cool-white character of the device. The distance to the Planckian locus is quantified by a Duv value of 0.0088, indicating a slight upward chromaticity shift toward the green-yellow region of the color space.

The color vector graphic provides detailed spatial insights into the localized hue shifts. It is Red and Warm Tone Desaturation (Bins 1, 15, and 16). The red test boundary (represented by the red line) shifts significantly inward relative to the black reference circle. This clear desaturation behavior in the red spectral band perfectly aligns with the previously identified negative R9 value, demonstrating a deficiency in rendering deep red objects.

In contrast, there is a Green-Yellow Enhancement (Bins 4, 5, and 6). The boundaries at bins 4, 5, and 6 show negligible displacement or match closely with the reference path. This indicates stable fidelity in the yellow-green region due to the dominant emission peak of the yellow phosphor centered around 545 nm.

Also, there is a Blue-Green Shifts (Bins 10 and 11). The vectors in the blue-green region indicate noticeable directional shifts, denoting subtle color distortions where blue-green shades may appear slightly altered under this lighting condition.

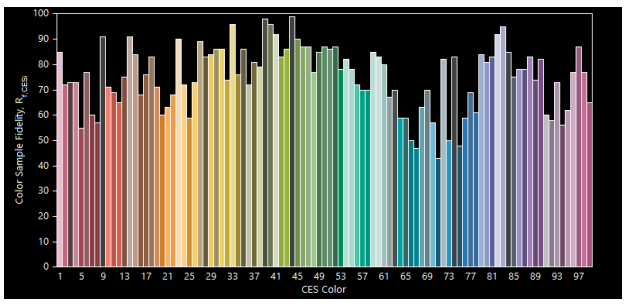


Fig. 8. Color Sample Fidelity ($R_{f,CESi}$) scores across the 99 Color Evaluation Samples (CES) of the IES TM-30-15 standard.

Figure 8 details the Color Sample Fidelity ($R_{f,CESi}$) scores across the 99 Color Evaluation Samples (CES) of the IES TM-30-15 standard, revealing distinct wavelength-dependent variations in the pc-WLED spectrum. Exceptional color rendering is achieved in the yellow-to-green regions (CES 29–53), with scores peaking between 90 and 99 due to the high spectral power density of the broad yellow phosphor emission. Conversely, moderate scores between 60 and 85 are maintained for earth tones and blue-purple hues (CES 13–28 and CES 77–99), sustained by the primary blue die emission. However, two distinct spectral deficiencies expose the limitations of the mono-phosphor architecture: a red deficiency (CES 1–12) where scores suppress to ~55, and a prominent cyan structural gap (CES 63–76) hitting a minimum valley of ~43 at CES 71, signifying an energy trough in the transition zone between the blue die emission and the yellow phosphor excitation slope.

4. DISSCUSION

For lighting application, the improvement of Ra should be conducted to increase its value close to value of 100. The lacking of red light in white light spectrum leads the low value of R9. It thus increased by combining with red phosphor. The value of Rf of 75 indicates the moderate color fidelity and a noticeable color shift may occur. In application requiring accurate color reproduction (e.g. art galleries, museums, retail display and photography), an Rf of 75 is insufficient and a higher Rf is generally preferred.

5. CONCLUSION

In summary, a high-conformity phosphor-converted white light-emitting diode (pc-WLED) was successfully fabricated utilizing an advanced, low-temperature ultraviolet (UV) radiation-curing compression molding process. Structural and morphological characterizations confirmed that the mechanical imprinting sequence achieved an exceptionally uniform, geometrically symmetric hemispherical yellow phosphor-resin matrix layer (6 wt%) covalently bonded directly over the primary InGaN blue LED dome. Electroluminescence characterization showed a well-balanced dual-peak spectrum composed of a sharp blue die emission peak (455 nm) and a broad yellow phosphor down-conversion envelope centered at 545 nm. Colorimetric

analysis under the CIE 1931 framework placed the output coordinates at (x= 0.32, y=0.38), aligning adjacent to the blackbody locus to generate a stable cool-white light with a CCT of 6164 K and a Duv of 0.0088. Color rendering evaluations revealed a traditional general color rendering index of 74 and an advanced IES TM-30-15 Fidelity Index Rf of 75. Granular analysis across the 99 Color Evaluation Samples (CES) and localized hue vectors showed near-optimal color rendering performance peaking up to 99 in the yellow-to-green bands, but exposed structural deficiencies in the deep-red R9= -25); CES 1–12 (approximate 55) and cyan spectral regions (CES 71 valley approximate 43). These results validate the high-efficiency, rapid-throughput capabilities of the UV-curing encapsulation method for solid-state lighting packages, while underscoring the future necessity of integrating narrow-band red or green emitting components to effectively eliminate structural energy troughs and achieve high-fidelity rendering applications.

REFERENCES

[1] S. Ye, F. Xiao, Y. X. Pan, Y. Y. Ma, and Q. Y. Zhang, "Phosphors in phosphor-converted white light-emitting diodes: Recent advances in materials, techniques and properties," *Mater. Sci. Eng. R Rep.*, vol. 71, no. 1, pp. 1–34, Dec. 2010, doi: 10.1016/j.mser.2010.07.001.

[2] A. G. Bispo-Jr., L. F. Saraiva, S. A. M. Lima, A. M. Pires, and M. R. Davolos, "Recent prospects on phosphor-converted LEDs for lighting, displays, phototherapy, and indoor farming," *J. Lumin.*, vol. 237, Art. no. 118167, Sep. 2021, doi: 10.1016/j.jlumin.2021.118167.

[3] E. F. Schubert and J. K. Kim, "Solid-state light sources getting smart," *Science*, vol. 308, no. 5726, pp. 1274–1278, May 2005, doi: 10.1126/science.1108712.

[4] A. de Almeida, B. Santos, P. Bertoldi, and M. Quicheron, "Solid state lighting review—Potential and challenges in Europe," *Renew. Sustain. Energy Rev.*, vol. 34, pp. 30–48, Jun. 2014, doi: 10.1016/j.rser.2014.02.029.

[5] C.-C. Sun *et al.*, "High uniformity in angular correlated-color-temperature distribution of white LEDs from 2800K to 6500K," *Opt. Express*, vol. 20, no. 6, pp. 6622–6630, Mar. 2012, doi: 10.1364/OE.20.006622.

[6] P. F. Smet, A. B. Parmentier, and D. Poelman, "Selecting conversion phosphors for white light-emitting diodes," *J. Electrochem. Soc.*, vol. 158, no. 6, pp. R37–R54, 2011, doi: 10.1149/1.3568524.

[7] J. J. Zhang, R. Hu, X. J. Yu, B. Xie, and X. B. Luo, "Spectral optimization based simultaneously on color-rendering index and color quality scale for white LED illumination," *Opt. Laser Technol.*, vol. 88, pp. 161–165, Feb. 2017, doi: 10.1016/j.optlastec.2016.08.006.

[8] L. Chen, C.-C. Lin, C.-W. Yeh, and R.-S. Liu, "Light converting inorganic phosphors for white light-emitting diodes," *Materials*, vol. 3, no. 3, pp. 2172–2195, Mar. 2010, doi: 10.3390/ma3032172.

[9] J. Qiao, J. Zhao, Q. Liu, and Z. Xia, "Recent advances in solid-state LED phosphors with thermally stable luminescence," *J. Rare Earths*, vol. 37, no. 6, pp. 565–572, Jun. 2019, doi: 10.1016/j.jre.2018.11.001.

[10] H. C. Yoon, K. Yoshihiro, H. Yoo, S. W. Lee, J. H. Oh, and Y. R. Do, "Low-yellowing phosphor-in-glass for high-power chip-on-board white LEDs by optimizing a low-melting Sn–P–F–O glass matrix," *Sci. Rep.*, vol. 8, Art. no. 7412, May 2018, doi: 10.1038/s41598-018-25680-6.

[11] J. Tian and W. Zhuang, "Thermal stability of nitride phosphors for light-emitting diodes," *Inorg. Chem. Front.*, vol. 8, no. 22, pp. 4933–4954, 2021, doi: 10.1039/D1QI00993A.

[12] P. Liu, C. She, L. Tan, P. Xu, and L. Yan, "Development of LED package heat dissipation research," *Micromachines*, vol. 13, no. 2, Art. no. 229, Jan. 2022, doi: 10.3390/mi13020229.

[13] C. Papatsimpa and J.-P. M. G. Linnartz, "Personalized office lighting for circadian health and improved sleep," *Sensors*, vol. 20, no. 16, Art. no. 4569, 2020, doi: 10.3390/s20164569.

[14] R. J. Lucas, S. N. Peirson, D. M. Berson, T. M. Brown, H. M. Cooper, C. A. Czeisler, M. G. Figueiro, P. D. Gamlin, S. W. Lockley, J. B. O'Hagan, L. L. A. Price, I. Provencio, D. J. Skene, and G. C. Brainard, "Measuring and using light in the melanopsin age," *Trends in Neurosciences*, vol. 37, no. 1, pp. 1–9, 2014, doi: 10.1016/j.tins.2013.10.004.

[15] M. S. Rea and M. G. Figueiro, "Light as a circadian stimulus for architectural lighting," *Lighting Research & Technology*, vol. 50, no. 4, pp. 497–510, 2018, doi: 10.1177/1477153516682368.

[16] C. Cajochen, S. Frey, D. Anders, J. Späti, M. Bues, A. Pross, R. Mager, A. Wirz-Justice, and O. Stefani, "Evening exposure to a light-emitting diodes (LED)-backlit computer screen affects circadian physiology and cognitive performance," *Journal of Applied Physiology*, vol. 110, no. 5, pp. 1432–1438, 2011, doi: 10.1152/japplphysiol.00165.2011.

[17] K. W. Houser, P. R. Boyce, J. M. Zeitzer, and M. Herf, "Human-centric lighting: Myth, magic or metaphor?" *Lighting Research & Technology*, vol. 53, no. 2, pp. 97–118, 2021, doi: 10.1177/1477153520958448.

[18] Q. Dai, W. Cai, L. Hao, W. Shi, and Z. Wang, "Spectral optimisation and a novel lighting-design space based on circadian stimulus," *Lighting Research & Technology*, vol. 50, no. 8, pp. 1198–1211, 2018, doi: 10.1177/1477153517733504.

[19] T. M. Brown, G. C. Brainard, C. Cajochen, C. A. Czeisler, J. P. Hanifin, S. W. Lockley, R. J. Lucas, M. Münch, J. B. O'Hagan, S. N. Peirson, L. L. A. Price, T. Roenneberg, L. J. M. Schlangen, D. J. Skene, M. Spitschan, C. Vetter, P. C. Zee, and K. P. Wright, Jr., "Recommendations for daytime, evening, and nighttime indoor light exposure to best support physiology, sleep, and wakefulness in healthy adults," *PLOS Biology*, vol. 20, no. 3, Art. no. e3001571, 2022, doi: 10.1371/journal.pbio.3001571.

[20] K. W. Houser and T. Esposito, "Human-centric lighting: Foundational considerations and a five-step design process," *Frontiers in Neurology*, vol. 12, Art. no. 630553, 2021, doi: 10.3389/fneur.2021.630553.